C. R. Mecanique 344 (2016) 355–374

Contents lists available at ScienceDirect

Comptes Rendus Mecanique

www.sciencedirect.com

Computational simulation of manufacturing processes

Simulation of shot peening: From process parameters to residual stress fields in a structure

Donato Gallitelli [a], Vincent Boyer [b], Maxime Gelineau [b], Yann Colaitis [a], Emmanuelle Rouhaud [a,*], Delphine Retraint [a], Régis Kubler [c], Marc Desvignes [c], Laurent Barrallier [c]

[a] Université de technologie de Troyes, ICD LASMIS, Troyes, France
[b] IRT M2P, Metz, France
[c] ENSAM ParisTech, MSMP, Aix-en-Provence, France

ARTICLE INFO

Article history:
Received 19 June 2015
Accepted 1 December 2015

Keywords:
Shot peening
Model
Residual stress
Shot dynamics

ABSTRACT

Manufacturing industries perform mechanical surface treatments like shot peening at the end of the manufacturing chain to protect important working parts. This treatment modifies the near surface of the treated part with the introduction of compressive residual stresses due to the repeated impacts of the shot. Then, the treated part exhibits, not only a longer life, but also a better fretting behavior, an improved resistance to corrosion… The objective of the present paper is first to study the relation between the process parameters and the material state (residual stress and plastic variables…) for a complex geometry. Next, a numerical tool is proposed, able to predict this material state in a time frame that is consistent with industrial constraints. The originality of the proposed approach thus consists in the chaining of the different steps. The first step is to choose the process parameters for the shot peening process considering conventional or ultrasonic shot peening and model the shot dynamics for a complex geometry. Once the impact velocity field is known, the objective is to compute the local incompatible plastic deformation field due to the repeated impacts using analytical methods. Then, a finite element model is used to compute the residual and deformation fields in the considered mechanical part. The complete method has been performed on the model of a gear, a mechanical part that is most often shot peened and exhibits a complex geometry.

1. Introduction

Most manufacturing industries routinely perform mechanical surface treatments at the end of the manufacturing chain to protect important working parts. Shot peening is probably the most common of these processes. The pioneering work of Almen [1] has indeed demonstrated the efficiency of shot peening processes to increase fatigue life, and this, for a very moderate cost. The treated part is in this case submitted to the impacts of many hard particles made of glass, ceramic or metal, known as the shot. The motion of the shot is produced with the help of turbines or compressed air in the

* Corresponding author.
E-mail address: rouhaud@utt.fr (E. Rouhaud).

http://dx.doi.org/10.1016/j.crme.2016.02.006

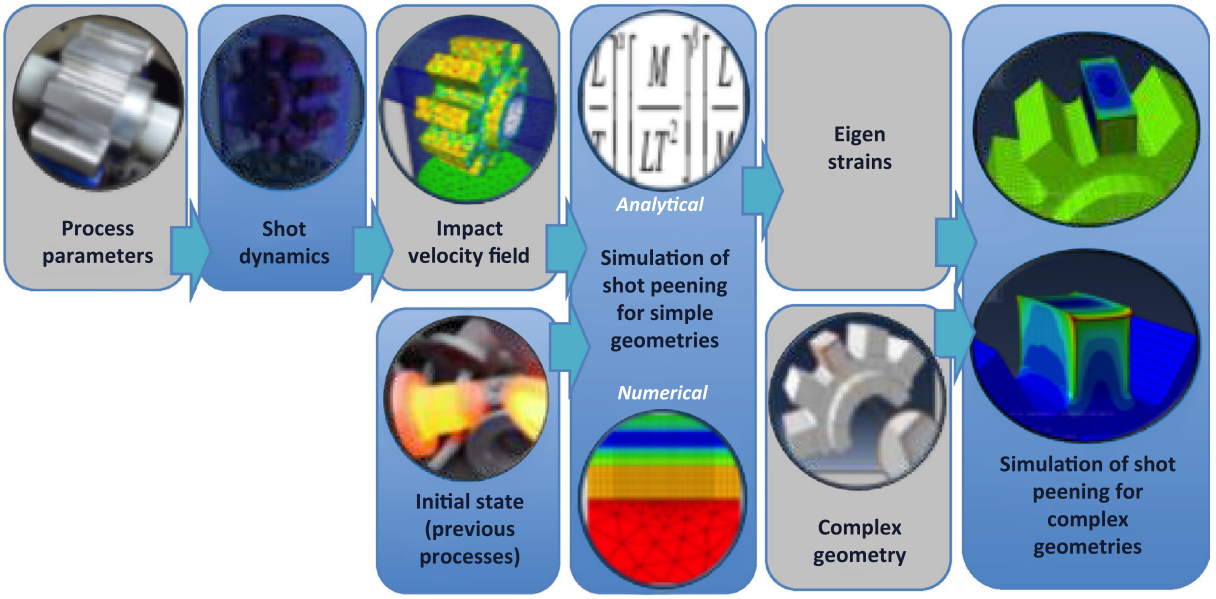

Fig. 1. Principle of the method with the chaining of different steps from the process parameters to the residual stress field in a complex geometry taking into account an initial state coming from previous manufacturing processes.

case of conventional shot peening or the vibrations of a sonotrode in the case of ultrasonic shot peening. This family of manufacturing processes modifies the near surface of the treated part with the introduction of compressive residual stresses and the modification of the structure of the material due to the repeated impacts. With an appropriate choice of process parameters, the treated part can exhibit, not only a longer life, but also a better fretting behavior, an improved resistance to corrosion…

Many parts in the aeronautical and automobile industries are shot peened. In most cases, the treatment is used to improve safety coefficients, but is not accounted for in design analyses. For the process to be taken into account at the design stage, the exact consequences of the parameters on the treated part have to be better mastered. This is further necessary for accreditation purposes in many industries. The hope is then to be able to reduce the weight of the mechanical parts, of crucial importance nowadays in transport industries. A renewed interest for pre-stressing processes has thus been observed recently. One of the objectives of the related modeling activity is to produce models that are efficient enough to enter design tools. It is thus important to understand the details of the physics at play. Then, the models should capture the essential phenomena at hand in the process and directly correlate process parameters with the consequences on the product. Furthermore, the time that is necessary to reach a solution has to be consistent with industrial constraints. Finally, in developing the models, one should keep in mind the fact that the results of the shot peening models are to be used as initial conditions for resistance or fatigue models and have to supply the appropriate data.

Proposed shot peening models are numerous in the literature and reviewed in [2–5]. Most of these models concentrate on the prediction of residual stress and plastic deformation fields and use the impact velocity as an initial condition and not the process parameters themselves. Moreover, the geometry of the treated part is most often reduced to a semi-infinite massif or to sufficiently thick plates. Nevertheless, it is clearly that the geometry of the part influences the treatment due to, for example, variations in the coverage of the impacts or the influence of boundaries on the mechanical fields.

The objective of the present paper is to propose methodologies able to produce a relation between the process parameters and the state of the treated part (stress field, hardening…) considering a complex geometry and including an initial state coming from previous manufacturing processes, this, in a time frame that is consistent with industrial constraints. Second-order phenomena will thus be neglected to simplify the model and analytical models preferred when possible. The existing methodologies proposed in the literature and suited to this specific objective are reviewed in this work. The originality of the proposed approach is thus to chain different steps, as detailed in Fig. 1, to relate the final state of the mechanical part after shot peening to the process parameters and this for a part with complex geometry. The first step is to choose the parameters considering conventional or ultrasonic shot peening and model the shot dynamics for a complex geometry. Once the velocity field of the impacts is known on the part, the objective is to compute the incompatible plastic deformation field due to the repeated impacts using numerical or analytical methods. Incompatible deformations due to other previous manufacturing processes may also be taken into account. Then, a finite element model is used to introduce the residual stress and deformation fields in a model of the mechanical part. The complete method is applied to the ultrasonic shot peening of a gear, a mechanical part that exhibits a complex geometry. Realistic (in other words industrial) conditions have been chosen for the process parameters to create a demonstrator for this methodology.

2. Mechanical state after shot peening

We wish first to concentrate on the mechanical state *after* shot peening with a review of the physical constraints and the technological data available in the literature. This analysis enables to select the preponderant phenomena to be selected and modeled in the next stage. In this section, we thus propose to review several hypotheses that can be made in the case of shot peening treatments taking the history of the part into account.

2.1. Mechanical problem

A residual stress field is a stress field that exists inside a part when no external load is applied to the system. The elastic strains are the sources of residual stresses in the part. It is here supposed that the material is isotropic and homogeneous and there is no plasticity induced by phase transformations at constant temperature. The residual stress tensor $\boldsymbol{\sigma}$ in a shot peened part of volume V and surface S of normal $\vec{\boldsymbol{n}}$ verifies:

$$\begin{cases} \operatorname{div}(\sigma) = 0 & \text{on } V \\ \sigma\vec{n} = 0 & \text{on } S \\ \sigma = E\left(\varepsilon - \varepsilon^{\mathrm{p}}\right) \end{cases} \tag{1}$$

assuming that the elastic behavior of the material is represented by the tensor modulus $\boldsymbol{E}$ representing Hooke's law; the total strain $\boldsymbol{\varepsilon}$ has been additively decomposed between an incompatible strain $\boldsymbol{\varepsilon^{\mathrm{p}}}$ and an elastic strain $\boldsymbol{\varepsilon^{\mathrm{e}}}$ ($\boldsymbol{\varepsilon} = \boldsymbol{\varepsilon^{\mathrm{e}}} + \boldsymbol{\varepsilon^{\mathrm{p}}}$) within a small strain framework. Residual stresses are due to strain heterogeneities introduced at any scale (macro- or microscopic scale). The main origin of residual stresses during mechanical treatments (shot peening, rolling) is the incompatibility of plastic strains [6]. In the case of nitriding, residual stresses are due to volume strains incompatibility caused by the diffusion/precipitation phenomena: insertion of nitrogen and carbon in the ferritic matrix as well as the formation of nitrides and carbides [7–9]. In the case of carburizing or carbonitriding, the diffusion and plastic strains incompatibility due to the differential expansion and the non-simultaneousness of phase transformations during the martensitic quenching actively contribute to the generation of residual stresses [10].

The possible evolution of residual stresses after mechanical loading is due to a re-plasticization of the material. As long as the structure remains in the elastic domain, neither the incompatible strains nor the existing residual stress state are modified. As a whole, residual stresses are due to incompatibilities in the deformation field. These incompatible deformations are also referred to as "stress-free strains" or "eigenstrains" following the work of Korsunsky [11].

2.2. Typical residual stress field after shot peening

It is possible to evaluate residual stresses after shot peening using different experimental methods such as incremental hole drilling methods or X-ray diffraction [12]. When the treatment has been homogeneous on a regular surface for which the local radius of curvature is large compared to the radius of the shot, the stress tensor can be approximated to take the following general form [3,13]:

$$\sigma \rightarrow \begin{pmatrix} \sigma(z) & 0 & 0 \\ 0 & \sigma(z) & 0 \\ 0 & 0 & 0 \end{pmatrix} \tag{2}$$

This tensor is expressed in the local coordinate system defined with the normal to the surface as presented in Fig. 2. A typical residual stress profile $\sigma(z)$ as it can be measured in shot peened parts is presented in Fig. 2. The value of the maximal compressive stress σ_{COMP} is usually observed to be below the yield stress σ_{y} of the material, but can reach higher values in the case of intensive shot peening treatments; in most cases, one has $0.8\sigma_{\mathrm{y}} < \sigma_{\mathrm{COMP}} < 1.2\sigma_{\mathrm{y}}$. The depth affected by the treatment, z_{AFF}, corresponding to the depth for which compressive stresses are observed, is usually of the order of 100 µm and is most often below 1 mm.

2.3. Relation between residual stresses and stress free strains for semi-infinite bodies

For a semi-infinite body, it is possible to establish an analytical relationship between residual stresses and stress-free strains keeping the same hypotheses as in Section 3.2. In this case, the total strain tensor takes the general form:

$$\boldsymbol{\varepsilon} \rightarrow \begin{pmatrix} 0 & 0 & 0 \\ 0 & 0 & 0 \\ 0 & 0 & \varepsilon_{zz}(z) \end{pmatrix}$$

This is established with the hypotheses made for the residual stresses in Section 3.2, added to the fact that, in a semi-infinite body, there is no possible in-plane displacements. The stress-free strain tensor then takes the form:

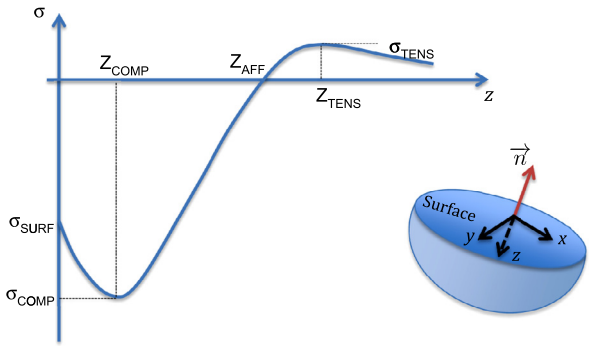

Fig. 2. Typical residual stress profile induced by shot peening.

$$\boldsymbol{\varepsilon^{p}} \rightarrow \begin{pmatrix} \varepsilon^{p}(z) & 0 & 0 \\ 0 & \varepsilon^{p}(z) & 0 \\ 0 & 0 & -2\varepsilon^{p}(z) \end{pmatrix}$$

assuming here that the plastic deformations, and thus the stress-free strains are isochoric. The elastic strains are the sources of residual stresses in the part. Using Hooke's law (E is Young's modulus and ν Poisson's ratio), and the fact that $\varepsilon^{e} + \varepsilon^{p} = 0$, it comes:

$$\varepsilon^{p}(z) = \frac{\nu - 1}{E}\sigma(z) \tag{3}$$

The analysis above is useful, because the hypotheses of a semi-infinite body can be made for most shot peened parts on a local basis. Indeed, in most cases, the treatment is homogeneous, the treated surface is regular and the depth affected by the treatment is small compared to the dimensions of the part. This can be verified by an experimental evaluation of the residual stress field. Eq. (3), first proposed by Zarka [14], is then useful in order to estimate the stress-free strain when the residual stress profiles are experimentally determined.

3. From process parameters to impact velocity field

3.1. Description of the model

Once the shot peening parameters are set using design and technological constraints, the first step is to determine the coverage and velocity of the impacts. It becomes important to predict the coverage in the case of complex geometries because the coverage may vary and this may eventually affect fatigue life [15]. The simulation of the shot dynamics as a function of the process parameters offers an answer to this problem. Three main methods have been proposed in the literature to reach this goal: the use of discrete elements software [16–20], the use of fluid simulation software [21], and the construction of a dedicated software [22–25]. In the case of shot dynamics, using an existing piece of software saves a lot of development time, but enables to reach, indeed, realistic solutions, with very long computation time. This is not compatible with industrial needs. Further, it is thus not possible to consider the shot dynamics around complex geometries, which is our original purpose. Therefore, we propose to consider a dedicated software.

The software proposed to model shot dynamics is able to consider industrial complex 3D geometries with the possibility to use a CAD software to construct the geometry of the part and process environment [23–25]. The motion of the part and a visualization of the shot motion around the part is possible (see Fig. 3). The model is based on models that have been initially created for granular gases [22]. The model predicts the complete trajectory of each individual sphere and in particular the data related to the impacts on the treated part. All collisions are detected, including the collisions between spheres and with the surrounding environment. Normal and tangential restitution coefficients, specific to each pair of colliding materials, enable us to take the behavior of the materials into account. It has been developed for ultrasonic and conventional shot peening. For conventional shot peening, Fig. 3 presents the shot flow and its local impacts on the part (located on the top of the figure, but not represented). A fictional box has been created around the impacted surface; outside of this box, the shot is recycled. For ultrasonic shot peening, Fig. 3 presents the shot around a gear. The sonotrode is represented in green at the bottom of the structure. The outside mesh represents the external wall of the ultrasonic chamber.

For both cases, it is then possible to predict and to validate the coverage and the location and impact velocity of each collision is known. Statistical studies may be performed to optimize the design of the process. The results are obtained in a reasonable time frame: for simple geometries, the computation is faster than the actual process itself. For complex geometries and a large amount of shot, when the actual process corresponds to several minutes, the computation can last for a few hours on a typical laptop computer and for very complex geometries like an entire turbine.

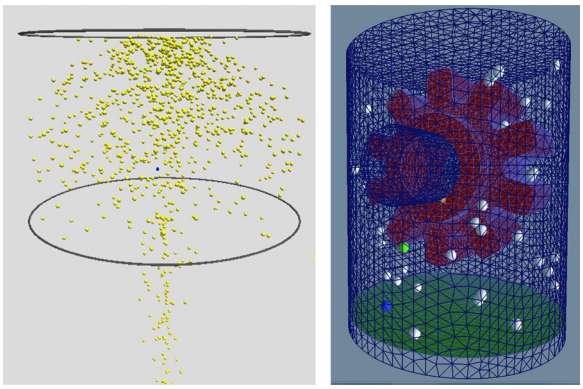

Fig. 3. Typical visuals obtained with the models for shot dynamics of conventional shot peening (left) and ultrasonic shot peening (right).

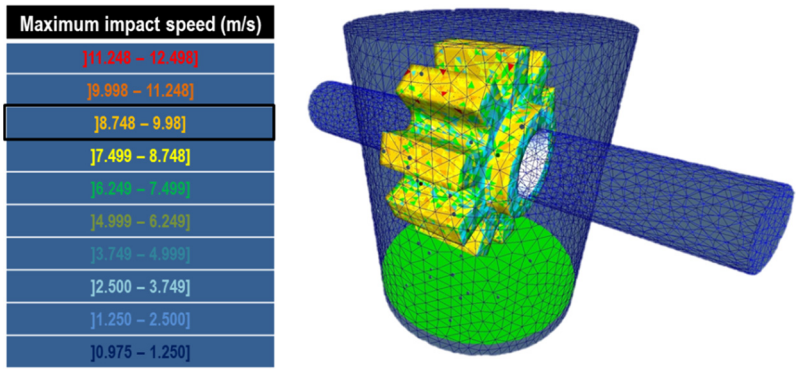

Fig. 4. Maximum impact speeds on a spur gear estimated by the shot dynamics model.

3.2. Case study and results

To validate the approach, we propose a case study and consider the ultrasonic shot peening of an aluminum (Al 7075 T7051) spur gear presented in Fig. 3 and apply the different models to obtain the residual stress field in the gear from the process parameters.

The following process parameters have been chosen:

- rotation of the gear with a speed of 10 rpm,
- shot: 100Cr6 steel beads (number of shots: 73; radius $R = 1.5$ mm, density $\rho_{\text{shot}} = 7800$ kg/m^3).
- Sonotrode: titanium (amplitude: 50 μm; frequency: 20 kHz).
- Duration of the treatment: 150 s.

The parameter of the material of the gear are: Young modulus $E = 70{,}000$ MPa, density $\rho_{\text{mat}} = 2700$ kg/m^3, yield stress $\sigma_y = 260$ MPa, and Poisson coefficient $\nu = 0.3$.

The computation of the shot dynamics takes a few minutes on a personal laptop computer. Form the saved data file, the local maximal normal impact speed has been extracted and is presented in Fig. 4. As a first approximation, it is considered that the maximal normal impact speed is most influent in terms of residual stress because these types of impacts lead to the most important local hardening and plastic deformation. On the external surfaces, the impact velocity field is quite homogeneous and can be considered constant with a value lose to $V = 10$ m/s. On the sides of the gear, for the surfaces that are always perpendicular to the sonotrode, the maximal normal impact speed is smaller and is considered equal to zero in the present study.

4. Simulation of shot peening for simple geometries

Models of shot peening are numerous in the literature. They are of three types: numerical, semi-analytical, and analytical. As far as numerical models of shot peening are concerned, the power of computers now enables us to reach a realistic solution in an acceptable amount of CPU time (several hours to a few days). Numerical models use finite elements to predict the state of a semi-infinite body after shot peening. Many models have been recently proposed considering a realistic number of impacts [26–29]. Various phenomena have been studied, like, for example, the microstructure of the material

[30] or the surface microgeometry [15]. Semi-analytical models have also been proposed [31]; these models reach realistic solution within a few hours of CPU time. Analytical models offer the advantage to propose a solution immediately.

The objective of this section is thus to detail two analytical methods to predict the residual stress field after shot peening when the velocity of the impact is known. The first method is based on dimensional analysis and the second is based on the hypothesis that the plastic effects have reached a stable cyclic state due to the repeated impacts. (In other words, each new impact at the same location generates a plastic loop identical to the loop generated by the previous impact.) The choice of the analytical methods is made here to accelerate the complete model of shot peening. Both methods have been tested for the prediction of the residual stress after conventional shot peening of an aluminum rod and compared to experimental data.

4.1. Dimensional analysis

A dimensional analysis approach [32] may be used to create an analytical model for the residual stress profile $\sigma(z)$ in a semi-infinite solid (Eq. (2)) [33–35]. The typical residual stress profile is approximated with a fourth-degree polynomial function such that:

$$\sigma(z) = a_0 + a_1 z + a_2 z^2 + a_3 z^3 + a_4 z^4$$

In this equation, the coefficients of the polynomial form depend on the five characteristic parameters described in Fig. 2, i.e. the surface compression stress σ_{SURF}, the maximal compression stress σ_{COMP}, the maximal tensile stress σ_{TENS}, the depth of maximal compression stress Z_{COMP} and the depth of maximal tensile stress Z_{TENS}.

It is considered that each one of these characteristic parameters depends on specific material properties and process-related parameters. These values can be established with a dimensional analysis approach using experimental and numerical results.

Based on physical considerations it is first necessary to define the input parameters that influence the most each of these characteristic parameters. We make the hypothesis that the five characteristic parameters σ_{SURF}, σ_{COMP}, σ_{TENS}, Z_{COMP} and Z_{TENS} depend on the following seven input parameters:

- parameters related to the shot: density ρ_{shot}, radius R, and maximal normal impact velocity V,
- parameters related to the shot peened part: density ρ_{mat}, Young's modulus E, yield stress σ_{y} and Poisson's ratio ν.

The results obtained with the shot dynamic model provide the velocity of the impact V. The other input parameters are known. Note that this step is essential and other parameters such as the local coverage could be entered in the analysis. This type of approach requires a strong expertise on the process to be efficient.

Then, it is possible to find the expression of a function F that describes the problem using the theorem π of Vaschy–Buckingham. This theorem says that if there is a relation between n physical variables such $a_0 = f(a_1, a_2, \ldots, a_{n-1})$, it is possible to write it as a relation between $n-k$ dimensionless numbers C_i of the form:

$$C_0 = F(C_1, C_2, \ldots, C_{n-k-1})$$

where n is the number of variables and k the number of dimensions. The function F is evaluated using experimental and/or numerical data.

We first apply this methodology to σ_{SURF}. With a technical expertise on the shot peening treatment [33], it can be shown that for σ_{SURF} (but also σ_{TENS} and σ_{COMP}) the important parameters to take into account are the shot velocity V and the material's characteristics $E\rho_{\text{mat}}$ and σ_{y}. According to the theorem, we have to find one relation between three non-dimensional numbers as C_0 and C_1. The non-dimensional numbers have to be defined with the different relevant parameters. We propose the following three parameters:

$$C_0 = \frac{\sigma_{\text{surf}}}{\sigma_{\text{y}}}, \qquad C_1 = \frac{E}{\sigma_{\text{y}}}, \qquad C_2 = V\left(\frac{\rho_{\text{mat}}}{\sigma_{\text{y}}}\right)^{\frac{1}{2}}$$

It is then possible to establish an analytical function $C_0 = g(C_1, C_2)$ to relate these three parameters using a set of experimental data. In other words, several experimental residual stress profiles have to be analyzed and the value of the residual stress on the surface is extracted for each profile. This has to be performed for different shot velocities and materials. Then the parameters C_0, C_1, and C_2 are evaluated for each case and presented in Fig. 5. A linear function is then established, representing the function g. It is hence necessary to possess a large amount of experimental data to obtain a realistic expression of this function. The difficulty is to obtain experimental data that will span a wide number of shot peening cases in terms of material and process parameters. The larger the number of points in Fig. 5, the better is the regression analysis to define the function between the non-dimensional numbers. The domain of validity of the model thus depends on the quantity of available experimental data and on the domain that it spans in terms of parameters (shot peened materials, different process parameters...).

The same methodology is applied to σ_{TENS}, σ_{COMP}, Z_{COMP} and Z_{TENS}. The result is a set of equations that gives the characteristic points of the residual stress profile:

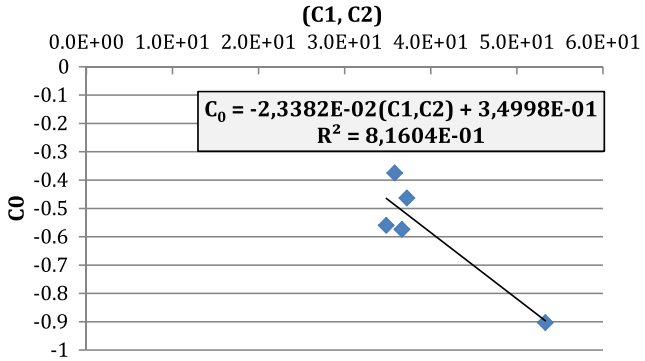

Fig. 5. Example $C_0 = g(C_1, C_2)$ using experimental data. Each point corresponds to a result extracted from experimental data [33].

$$\sigma_{\text{SURF}} = \left[-2.3382 \cdot 10^{-2}\left(\frac{E}{\sigma_y}\right)V\left(\frac{\rho_{\text{mat}}}{\sigma_y}\right)^{\frac{1}{2}} + 3.4998 \cdot 10^{-1}\right]\sigma_y$$

$$\sigma_{\text{COMP}} = \left[-1.7088 \cdot 10^{-2}\left(\frac{E}{\sigma_y}\right)V\left(\frac{\rho_{\text{mat}}}{\sigma_y}\right)^{\frac{1}{2}} - 1.1635 \cdot 10^{-1}\right]\sigma_y$$

$$\sigma_{\text{TENS}} = \left[23.367\left(\frac{\sigma_y}{E}\right)V\left(\frac{\rho_{\text{mat}}}{\sigma_y}\right)^{\frac{1}{2}} + 5.6326 \cdot 10^{-2}\right]\sigma_y$$

$$Z_{\text{COMP}} = \left[4256 \cdot 10^{-1}\left(\frac{\delta}{R}\right)^{1/4}\left(V\left(\frac{\rho_{\text{mat}}}{\sigma_y}\right)^{\frac{1}{2}} + \frac{4\pi}{17}\right) + 1.8324 \cdot 10^{-3}\right]R$$

$$Z_{\text{TENS}} = \left[1.5574\left(\frac{\delta}{R}\right)^{2/5}\left(V\left(\frac{\rho_{\text{mat}}}{\sigma_y}\right)^{\frac{1}{2}} + \frac{4\pi}{17}\right) + 4212 \cdot 10^{-2}\right]R$$

with

$$\delta = \left[7.2091\left(V\left(\frac{\rho_{\text{mat}}}{\sigma_y}\right)^{\frac{1}{2}}\right) + 1.1918\right]R\left(\frac{5\pi\rho_{\text{shot}}V^2(1-\nu^2)}{4E}\right)^{\frac{2}{5}}$$

The residual stress field in a shot-peened rod made of aluminum has been computed with this dimensional analysis model and is compared with experimental results taken from [36], as presented in Fig. 6. The treatment is conventional shot peening. Clearly, the model captures some of the features of the experimental profile (maximal compressive stresses) and could be improved if a larger number of experimental data were available to construct the regression presented in Fig. 5.

Thus, when the non-dimensional numbers have been properly identified, the equations above lead to the general form of the residual stress profile in any cases, within the hypotheses of this work. The model is completely analytical and may be implemented on data sheet software. The difficulty with this analysis is that it requires expertise on the process and a large number of experimental data to be valid. But once it has been performed, it gives an interesting solution to produce the residual stress and works best when identified with experimental data only on one material with several process parameters. Because the shot-peened object is a semi-infinite solid, it is possible to analytically deduce the plastic deformation field that is associated with the computed residual stress field as presented in Section 4.2.

4.2. Simplified elastoplastic model for structure analysis

The global aim of this method, first developed by Zarka et al. [14], is to model the elastoplastic state of a structure once it has reached a stable state during cyclic loading. The method is based on cyclic analysis of mechanical structures and the analysis is made once cycles have reached a steady state. The method is thus limited to elastic and plastic shakedown, and is not able to describe ratcheting effects. It has been shown that in this case, an elastic solution of the problem enables us to compute the steady-state solution. This theory has been successfully applied to conventional shot peening of a semi-infinite body to create an analytical model of the process [37]. In the case of ultrasonic shot peening, the diameter of the shot and the impact velocities are larger, the number of impacts in one area is also smaller, such that the method is better suited for conventional shot peening. In this case, it consists in assuming that cyclic fields are established with the repeated impacts of the shot and that a steady state is eventually reached. The fundamental idea is to introduce transformed parameters, calculated from internal parameters of the structure, leading to a simple treatment of the yield criterion.

To compute the elastic stress tensor $\boldsymbol{\Sigma}^{\mathbf{el}}$, the elastic theory of Hertz is used for a frictionless contact between a rigid sphere and an elastic semi-infinite body. The solution is limited to the solution at the level of the axis of symmetry of the problem with:

$$\boldsymbol{\Sigma}^{\mathbf{el}} \to \begin{pmatrix} \Sigma^{\mathrm{el}} & 0 & 0 \\ 0 & \Sigma^{\mathrm{el}} & 0 \\ 0 & 0 & \Sigma^{\mathrm{el}}_{zz} \end{pmatrix}$$

$$\Sigma^{\mathrm{el}} = P_0(1+\nu)\left(\frac{z}{a}\tan^{-1}\left(\frac{a}{z}\right) - 1\right) + P_0\left(\frac{a^2}{2(a^2+z^2)}\right)$$

$$\Sigma^{\mathrm{el}}_{zz} = -P_0\left(\frac{a^2}{2(a^2+z^2)}\right)$$

where a is the radius at maximal penetration of the shot and P_0 the maximal pressure during contact. These two parameters can be expressed analytically with the incoming speed of the shot V obtained with the shot dynamic model:

$$a = R\left(\frac{5\pi\rho_{\mathrm{mat}}(1+\nu^2)}{4E}V^2\right)^{1/5}$$

$$P_0 = \frac{2E}{\pi R(1+\nu^2)}a$$

After several impacts, the material reaches a steady state, the load Σ can be decomposed into two terms:

$$\boldsymbol{\Sigma} = \boldsymbol{\Sigma}^{\mathbf{el}} + \boldsymbol{\sigma}$$

where σ is the residual stress field due to shot peening. For the inelastic deformation tensor, we can also write:

$$\boldsymbol{\varepsilon}^{\mathbf{ine}} = \boldsymbol{M}\boldsymbol{\sigma} + \boldsymbol{\varepsilon}^{\mathbf{p}}$$

where $\boldsymbol{M}$ is the elastic compliance tensor, and $\boldsymbol{\varepsilon}^{\mathbf{p}}$ is the plastic deformation tensor. The elastic equivalent stress to define the yield criteria is further defined as:

$$\Sigma^{\mathrm{el}}_{\mathrm{eq}} = \sqrt{2/3}\left(\Sigma^{\mathrm{el}} - \Sigma^{\mathrm{el}}_{zz}\right)$$

A transformed parameter Y is introduced that depends on a global "irreversible" deformation mechanism α (instant plasticity, linear viscoelasticity and viscoplasticity) such that:

$$\boldsymbol{Y} = \boldsymbol{\alpha} - \mathrm{dev}(\boldsymbol{\sigma})$$

where the plastic part of the material is assumed to have a kinematic linear hardening behavior (the hardening parameter will be noted h) and:

$$\alpha = \frac{3}{2}h \cdot E^{\mathrm{p}}$$

The yield criterion is defined such that:

$$\frac{1}{2}\left(\mathrm{dev}\left(\Sigma^{\mathrm{el}}\right) - Y\right)^{\mathrm{T}}\left(\mathrm{dev}\left(\Sigma^{\mathrm{el}}\right) - Y\right) - \sigma_{\mathrm{y}}^2 < 0$$

In the space of transformed parameters, the description of plastic behavior consists of a translation of a sphere of radius $\sqrt{\frac{2}{3}}\sigma_{\mathrm{y}}$, the center of which follows the direction given by $\mathrm{dev}(\Sigma^{\mathrm{el}})$. The parameter Y is then calculated by analyzing the mechanical state of the structure. Three cases are possible:

1) $\Sigma^{\mathrm{el}}_{\mathrm{eq}} < \sqrt{\frac{2}{3}}\sigma_{\mathrm{y}}$: the load remains in the elastic domain of the structure, and Y remains unchanged.
2) $\Sigma^{\mathrm{el}}_{\mathrm{eq}} > \sqrt{\frac{2}{3}}\sigma_{\mathrm{y}}$: the structure undergoes plastic deformation, but the initial and final position of the yield criterion share a non-void domain. In this case, Y is the normal projection of its initial position on the boundary of the common domain and:

$$Y = \frac{\Sigma^{\mathrm{el}}_{\mathrm{eq}} - \sqrt{\frac{2}{3}}\sigma_{\mathrm{y}}}{\sqrt{6}}$$

3) $\Sigma^{\mathrm{el}}_{\mathrm{eq}} > 2\sqrt{\frac{2}{3}}\sigma_{\mathrm{y}}$: there is no common domain between the initial and final positions of the yield criterion. In this case Y is the normal projection of its initial position on the boundary of the unloaded domain and:

$$Y = \frac{\Sigma^{\mathrm{el}}_{\mathrm{eq}}}{\sqrt{6}}$$

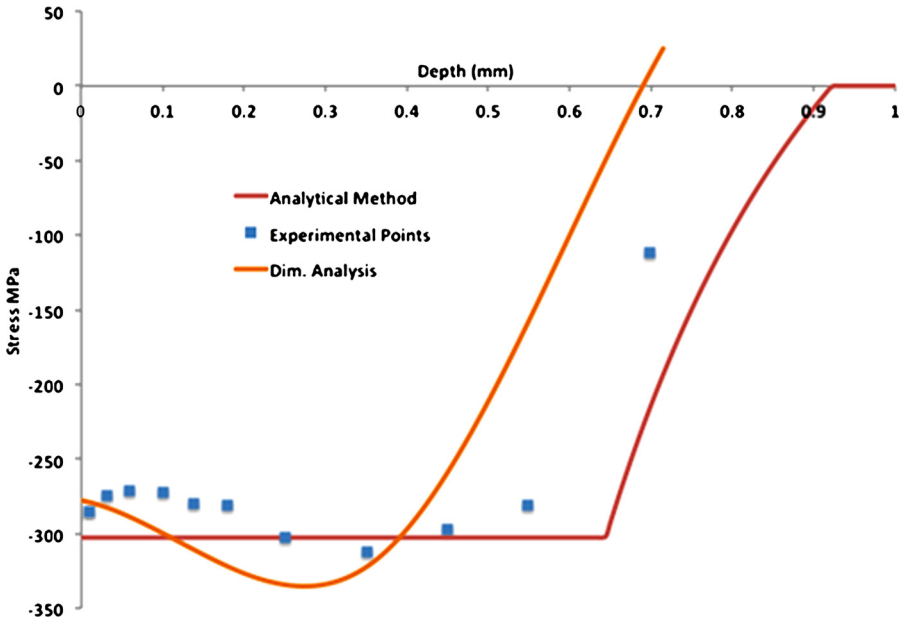

Fig. 6. Residual stress in a shot-peened rod made of aluminum (yield stress $\sigma_y = 310$ MPa and hardening slope $h = 1200$ MPa). The models correspond to the dimensional analysis presented in Section 4.1 (orange line) and to the analytical model presented in Section 4.2 (red line). The experimental data is presented with blue squares [36]. The shot peening parameters are $V = 80$ m/s for the shot velocity and $R = 0.45$ mm for the steel shot radius.

Finally, in the case of a semi-infinite body with Eq. (3), we have:

$$\varepsilon^{\mathrm{p}}(z) = Y(z)\left(\frac{3(1-\nu)}{2h(1-\nu)+E}\right)$$

It is then possible to compute a residual stress field in an aluminum shot-peened rod, and the result is presented in Fig. 6. This result is compared with the experimental data presented in [36] and with the result obtained in Section 4.1 using dimensional analysis. The treatment is conventional shot peening. To respect the hypothesis of the method, it is important to verify the fact that the material has reached a steady state corresponding to a high impact coverage. This is most often reached for conventional shot peening. The predictions of this model are clearly in good agreement with the experimental results. Next, on a predictive context, the model has been applied to compute the residual stress field for the gear treated with ultrasonic shot peening and corresponding to the studied case described in Section 2.2. The result is presented in Fig. 7. The objective is to introduce this profile in the model of the gear as described in Section 6.

The model is again completely analytical and may be implemented on data sheet software. This method, developed when computer capacities were limited, proposes a very efficient and accurate way to calculate residual stress induced by shot peening. Although satisfactory for materials exhibiting strong work hardening behavior, experiment and model are quite different in the case of BBC materials, especially nickel alloys. Many improvements have been proposed since. Slim [38] studied the cyclic behavior of the infinite body to introduce an estimate of the coverage in the model. Khabou [39] introduced two coupled mechanisms able to describe correctly the nonlinear evolution of stress during the early stages of plasticity.

5. Introducing a residual stress field in a finite-element model

As established in Section 3, for a uniform surface treatment on a regular thick piece, it can be considered that the part is a semi-infinite body locally. The residual stresses may be experimentally evaluated or predicted with a given model or simulation. It is next possible to deduce the corresponding stress free strains from the residual stresses considering that the part is a semi-infinite body. Then, it is possible to introduce these fields into more complex geometries. Residual stresses result from an overall balancing of the structure in order to comply with the compatibility equations, boundary conditions, and equilibrium equations. These stresses thus strongly depend on the geometry. This is not the case for the stress-free strains, which mainly depend on the material state. These incompatible strains can thus be introduced as initial conditions of an elastic computation to obtain the model for a shot-peened mechanical part. This is possible even if the geometry of the part is not a semi-infinite body. Several methods have been developed to introduce these stress-free strains, two of which are reviewed in the present Section.

The methodologies developed below may be used to introduce a residual state due to shot peening, but also to introduce an initial state to take into account previous manufacturing processes and combine their effects with shot peening. The objective of this section is thus twofold.

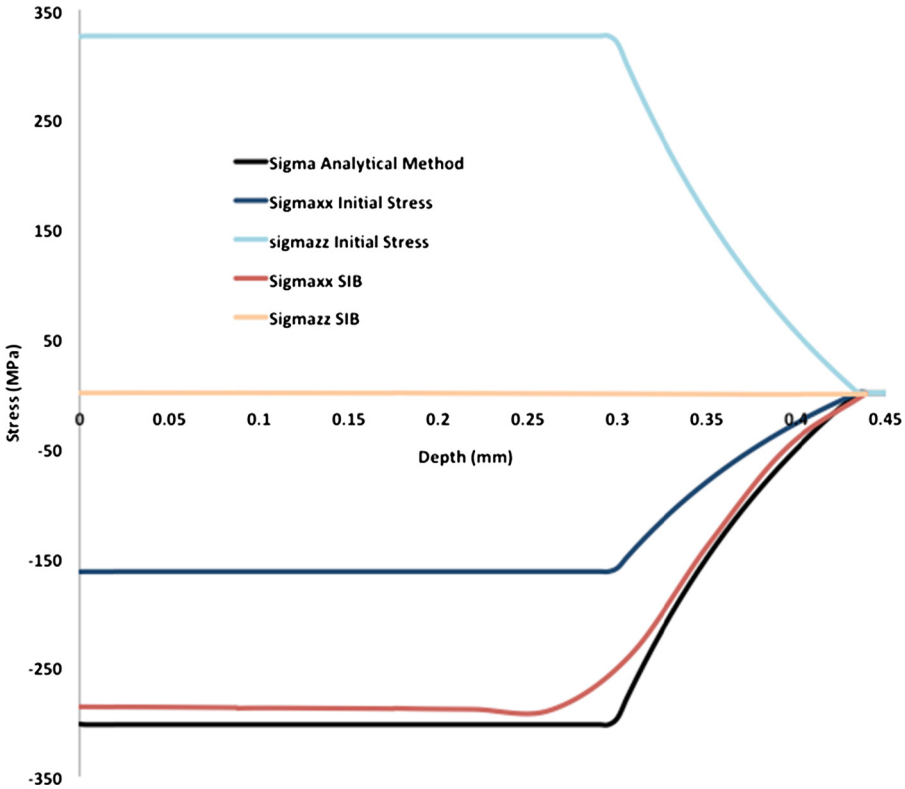

Fig. 7. Residual stress within a semi-infinite solid due to the ultrasonic shot peening of an aluminum rod in the conditions described in Section 2.2 computed with the analytical method (thick black line). Initial stress field computed for the above case (σ^0 thin dark blue, σ^0_{zz} thin light blue). Corresponding residual stress values computed after the introduction of this initial stress field in a finite-element model of a cube that can be assimilated to a semi-infinite body (SIB) (red line for σ_{xx} and orange line for σ_{zz}).

5.1. Initial fields

Depending on the options offered by the finite-element software, it is possible to introduce the plastic deformation field or the stress field as initial conditions. The stress-free strains computed in the previous sections can be used as an initial plastic deformation field. If the initial stress field is chosen, it is necessary to compute the initial stress field corresponding to the stress-free strain and that will lead to the residual stress field after equilibrium in order to ensure a coherent deformation field [40]. This field $\boldsymbol{\sigma^0}$ is evaluated from the residual stress field $\boldsymbol{\sigma}$ to be introduced, considering that the total deformations are equal to zero in Eq. (1). This corresponds to a field that is imposed before the initial increment in the finite-elements computation. This leads to:

$$\sigma^0(z) = -\frac{\sigma^0_{zz}(z)}{2} = \left(\frac{1-\nu}{1+\nu}\right)\sigma(z) \quad \text{with } \overline{\overline{\boldsymbol{\sigma^0}}} = \begin{pmatrix} \sigma^0 & 0 & 0 \\ 0 & \sigma^0 & 0 \\ 0 & 0 & \sigma^0_{zz} \end{pmatrix} \tag{4}$$

The method has been applied to a model of semi-infinite body for validation and to the study case of the gear. The residual stress field in a semi-infinite body has first been computed using the analytical method described in Section 4.2. It has been computed for the ultrasonic shot peening following the conditions and parameters of the study case of the gear as described in Section 2.2; the result is presented in Fig. 7. The initial stress field is next computed with Eq. (4). The nonzero components of this initial stress tensor are presented in Fig. 7 in blue as a function of the depth.

As a validation test, this initial stress in next introduced in a finite element model of a semi-infinite body: a cube with a 50-mm side length composed of the same material as the gear and the resulting residual stress field after equilibrium is presented in Fig. 7 with red and orange lines. The profile represented in red is very close to the one that has been computed analytically in the semi-infinite body. Note that the component σ_{zz} is indeed equal to zero after equilibrium. The difference comes from the fact that the part in which it has been introduced is not strictly speaking an infinite body but a large massif.

5.2. Fictitious thermal loading method

Ahdad and Desvignes [41] proposed a method to introduce residual stresses in a finite element code. In this case, the plastic strain field is generated by a homogeneous fictitious thermal loading $\Delta\theta^*$, with fictitious thermal expansion

coefficients $\alpha^*(z)$ depending on the depth z that has to be consistently determined. Dealing either with shot peening or with thermomechanical treatments, stress-free strains ε^{f} are in fact divided into a plastic strain and a volumetric strain ε^{v} of thermal or metallurgical origin:

$$\varepsilon^{\mathrm{f}}(z) = \varepsilon^{\mathrm{p}}(z) + \varepsilon^{\mathrm{v}}(z)$$

For a purely mechanical treatment such as shot peening, the volumetric strains are negligible (i.e. $\varepsilon^{\mathrm{v}} = 0$) and the plastic strain tensor may be evaluated from the experimental residual stresses according to Eq. (3). First, the case of an infinite body with no displacement submitted to a temperature change is considered. Upon application of a global temperature change $\Delta\theta^*$, a plastic strain field is generated when the equivalent stress reaches the yield strength σ_{y}, and evolves according to the hardening behavior. We first establish the relationship between the plastic strain $\varepsilon^{\mathrm{p}}(z)$ and the thermal expansion coefficients $\alpha^*(z)$ inducing it. It is supposed that the material is elastically isotropic and that it presents an elastoplastic behavior with linear kinematic hardening. It is further supposed that the material is not homogeneous: the Lamé coefficients λ and μ depend on the depth z. If the surface of a semi-infinite body is treated, the total strain is zero and:

$$\varepsilon(z) = \varepsilon^{\mathrm{e}}(z) + \varepsilon^{\mathrm{p}}(z) + \varepsilon^{\mathrm{th}^*}(z) = 0 \tag{5}$$

where $\varepsilon^{\mathrm{th}^*}(z) = \alpha^*\Delta\theta^*$ represents a fictitious thermal strain tensor induced by a fictitious temperature change $\Delta\theta^*$. The calculation of the stress at each depth z is then:

$$\sigma(z) = 2\mu(z)\cdot\varepsilon^{\mathrm{e}}(z) + \lambda(z)\cdot\mathrm{Tr}\big(\varepsilon^{\mathrm{e}}(z)\big)\cdot I \tag{6}$$

Inserting Eq. (5) in Eq. (6), the stress field is written as:

$$\sigma(z) = 2\mu(z)\cdot\big(-\varepsilon^{\mathrm{p}}(z) - \varepsilon^{\mathrm{th}^*}(z)\big) + \lambda(z)\cdot\mathrm{Tr}\big(-\varepsilon^{\mathrm{p}}(z) - \varepsilon^{\mathrm{th}^*}(z)\big)\cdot I \tag{7}$$

Since $\mathrm{Tr}(\varepsilon^{\mathrm{p}}) = 0$, Eq. (7) becomes:

$$\sigma(z) = 2\mu(z)\cdot\big(-\varepsilon^{\mathrm{p}}(z) - \varepsilon^{\mathrm{th}^*}(z)\big) + \lambda(z)\cdot\mathrm{Tr}\big(-\varepsilon^{\mathrm{th}^*}(z)\big)\cdot I \tag{8}$$

In order to obtain the plastic strain field, the von Mises yield criterion is applied with a fictitious linear kinematical hardening, arbitrarily chosen to calculate the fictitious thermal expansion coefficients. The yield criterion is given by:

$$\big(\mathrm{dev}(\sigma) - X\big) : \big(\mathrm{dev}(\sigma) - X\big) = \frac{2}{3}\sigma_{\mathrm{y}}^2 \quad \text{with } X = 2/3h\cdot\varepsilon^{\mathrm{p}} \tag{9}$$

where $\mathrm{dev}(\sigma)$ is the deviatoric part of the stress tensor, X is the kinematical stress tensor and h is the hardening slope. By inserting Eq. (8) into Eq. (9), the following expression is obtained:

$$\mathrm{Tr}\Big[\big(\mathrm{dev}\big(-2\mu(z)\cdot\varepsilon^{\mathrm{th}^*}\big) - \big(2\mu(z) + C\big)\cdot\varepsilon^{\mathrm{p}}\big)^2\Big] = \frac{2}{3}\sigma_{\mathrm{y}}^2 \tag{10}$$

Since the thermal strain $\varepsilon^{\mathrm{th}^*}$ is purely fictitious in the presented case, a variable K is defined to solve Eq. (10), such as:

$$K(z)\cdot\varepsilon^{\mathrm{p}} = -2\mu(z)\cdot\varepsilon^{\mathrm{th}^*}(z) - \big(2\mu(z) + C\big)\cdot\varepsilon^{\mathrm{p}} \tag{11}$$

Combining Eqs. (10) and (11), K is given by:

$$\big|K(z)\big| = \left|\frac{\sigma_{\mathrm{y}}}{3\cdot\varepsilon_{xx}^{\mathrm{p}}(z)}\right|$$

Finally, from the plastic strain tensor calculated from the experimental stress profile using Eq. (3) and with $\varepsilon^{\mathrm{th}^*}(z) = \alpha^*(z)\Delta\theta^*$, the fictitious thermal expansion coefficients are determined from Eq. (11) as:

$$\alpha^*(z) = -\frac{2\mu(z) + C + K(z)}{2\mu(z)\cdot\Delta\theta^*}\cdot\varepsilon^{\mathrm{p}}(z) \tag{12}$$

which proves that the fictitious thermal strain tensor is a deviatoric tensor.

To illustrate the fictitious thermal loading method and compare it to the one obtained by applying initial fields in a commercial finite element code like ABAQUS, Renaud et al. [42] investigated the case of a parallelepiped massif with dimensions of $2 \times 2 \times 2$ mm^3 in the case of a mechanical treatment of shot peening and in the case of a thermochemical treatment (see section 6.1). For semi-infinite boundary conditions, the displacements normal to all surfaces except to the top one are constrained as illustrated in Fig. 8. All the profiles presented in this section are plotted along the z direction starting from point A. The mesh consists of linear brick elements of size varying from $0.2 \times 0.2 \times 0.03$ mm^3 close to the surface to $0.2 \times 0.2 \times 0.2$ mm^3 far from the surface.

The procedure is applied with the residual stress profile determined by X-ray diffraction on a shot peened steel as presented in Fig. 9 (shot peening parameters: Almen intensity F51A, 600 µm steel shot and a coverage of 110%). The plastic strain field is calculated from the residual stresses using Eq. (3) in the case of a semi-infinite massif. The fictitious thermal

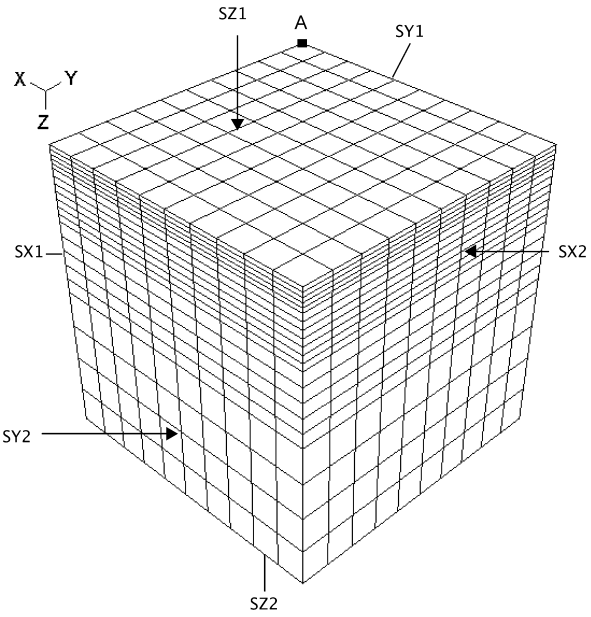

Fig. 8. Mesh of the semi-infinite media. The normal displacements are blocked for the surfaces SX1, SX2, SY1, SY2 and SZ2. Profiles are plotted along direction z starting from node A.

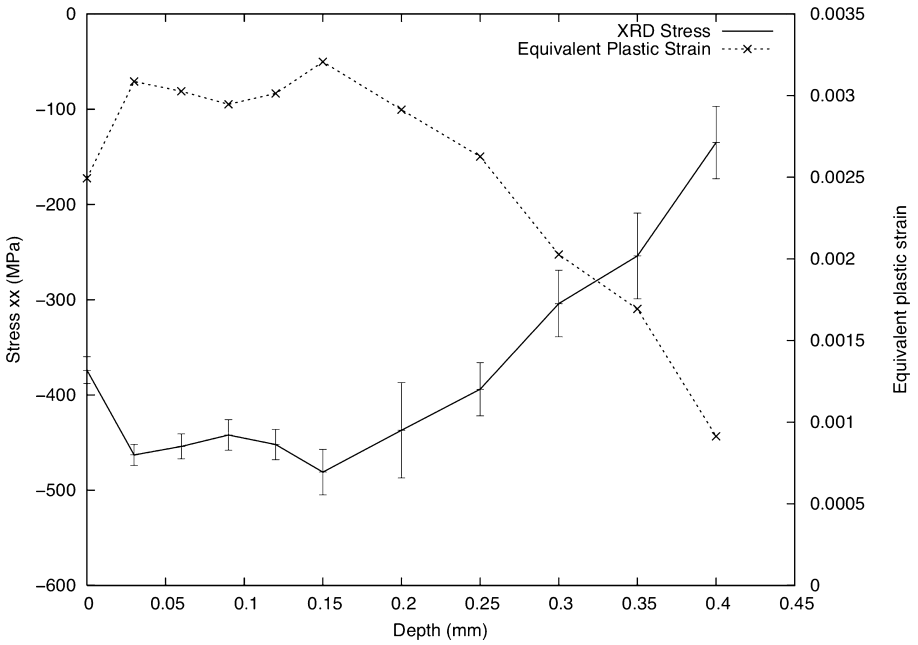

Fig. 9. Shot peened specimen with an Almen intensity of F51A and a coverage ratio of 110% using 0.6 mm diameter shot. Residual stresses determined by X-ray diffraction. Corresponding plastic strains (Eq. (3)).

expansion coefficients for each depth are calculated using Eq. (12) under a fictitious temperature variation $\Delta\theta^* = 100\,^\circ\mathrm{C}$. All the elements have the same elastic isotropic properties $E = 210$ GPa and $\nu = 0.3$, with a yield strength $\sigma_y = 760$ MPa and a hardening slope $h = 5$ GPa. The degrees of freedom of all nodes of the model are blocked and the fictitious temperature change of $100\,^\circ\mathrm{C}$ is applied. The degrees of freedom of all nodes are then released with the exception of the one needed for semi-infinite boundary conditions. The thermal stresses are finally removed by canceling the effect of the fictitious temperature load, i.e. $\theta^* = 0\,^\circ\mathrm{C}$.

The experimental stress profile and the calculated strain profile are also implemented directly in each element as initial conditions for comparison. Fig. 10 illustrates the fact that this method leads to the same stress and plastic strain profiles

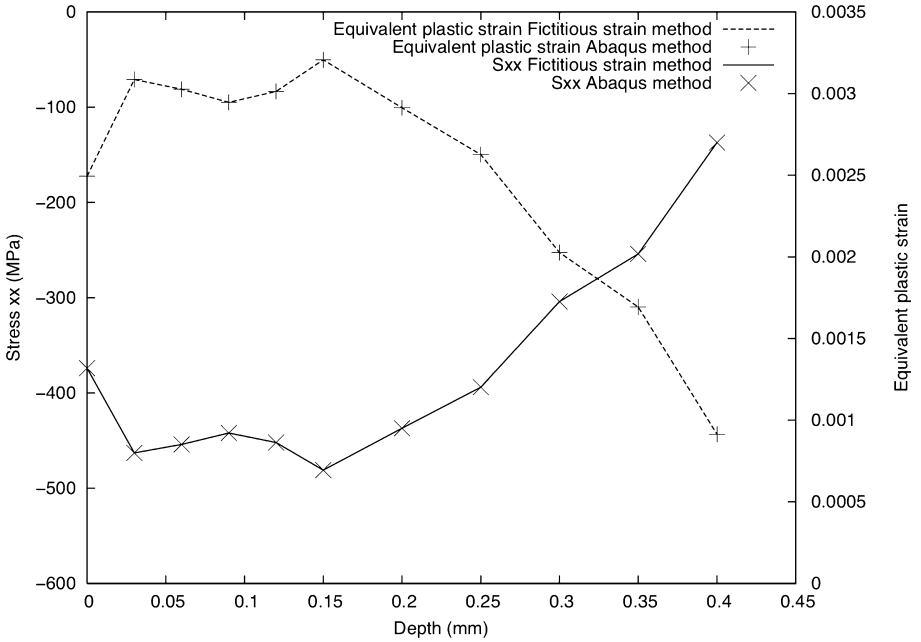

Fig. 10. Comparisons between the fictitious strain method and the introduction of the residual stress field as an initial condition for the shot peened semi-infinite case (F51A).

as for the fictitious thermal strain method. The main advantage of the latter is that it enables us to also establish an initial value for the internal variables, like the hardening state.

6. Residual stress field due to shot peening for complex cases

To complete the chains, the methods that have been detailed in the previous Sections are now combined and applied to complex cases. We will consider the case of shot peening after thermochemical treatments to validate the introduction of an initial state before shot peening and shot peening of a part with a complex geometry.

6.1. Shot peening after thermochemical treatments

The simulation of shot peening after a thermochemical treatment proceeds in two sequential steps:

1. Generation of the initial mechanical state induced by the thermochemical treatment (residual stress, hardening, metallurgical transformation).
2. Simulation of shot peening (sequential impacts of sphere with finite element analysis).

Renaud [42] simulated the generation of an initial mechanical state induced by a thermochemical treatment (carburizing and carbonitriding). The difficulty arises from:

– a preexisting gradient of material behavior from the surface to the core of the material,
– a gradient of thermo-metallurgical volumetric strain ε^{v} superimposed to the plastic strain induced by the treatment where carbon and nitrogen diffusion takes place.

First, the mechanical behavior is estimated at each depth from the tensile curve of the non-treated material (core) and the hardness profile of the treated component (see Fig. 11). Thermo-metallurgical strains are obtained experimentally using dilatometric tests. JMatPro software can be used in order to estimate the thermo-metallurgical strain at each depth with the carbon and nitrogen profiles, the phase proportion for a given chemical composition as a function of temperature during the quenching process [43,44]. Fig. 12 presents examples of dilatometric tests provided by JMatPro software, in the core of the part (with 0.29% C) and near the surface (with a composition of 0.85% C and 0.3% N). Phase transformations first take place in the core, because the martensite starting temperature is higher in the core than on the surface due to the chemical gradient. As a result of the studied carbonitriding treatment, Fig. 13 presents the in-depth thermo-metallurgical strain profiles ε^{v} depending on carbon and nitrogen contents at 25 °C obtained with JMatPro software.

Once the thermo-metallurgical volumetric strain ε^{v} is obtained, the induced plastic strain can be calculated from Eq. (3) such as:

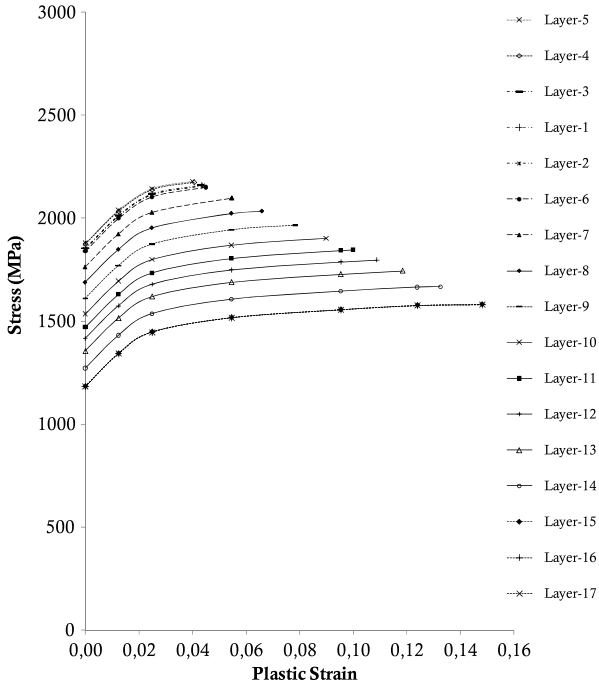

Fig. 11. Hardening behavior of different layers of a carbonitrided part.

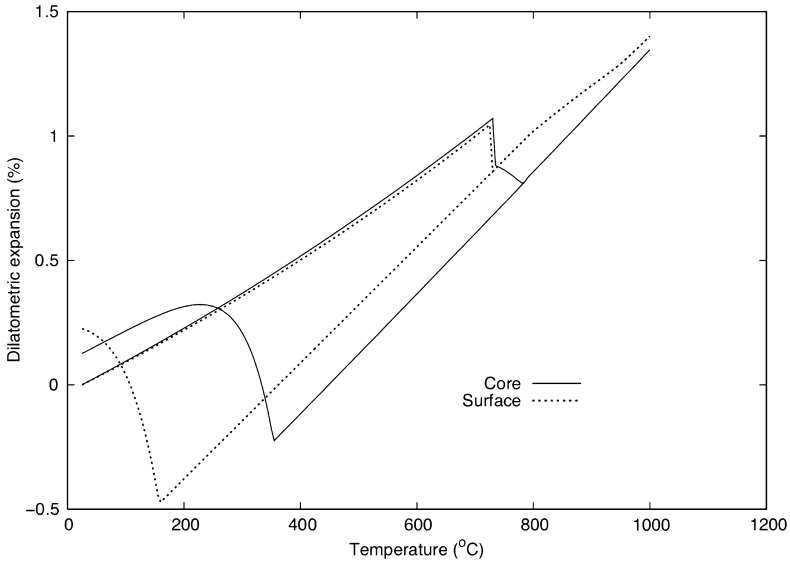

Fig. 12. Dilatometric expansion curves obtained with JMatPro. 29MnCr5 steel grade with a composition of 0.29%wt C in the core of the material and 0.85%wt C – 0.3%wt N near the surface.

$$\varepsilon^{\mathrm{p}}(z) = \frac{\nu - 1}{E}\sigma(z) - \varepsilon^{\mathrm{v}}(z)$$

Fig. 14 presents the equivalent plastic strain profile calculated. This figure compares the equivalent plastic strain profile calculated with and without considering the thermo-metallurgical strain. The maximum of the equivalent plastic strain is closer to the surface when the thermo-metallurgical volumetric strain is taken into account. For a thermochemical treatment, the initial mechanical state is described by the stress–strain curves in Fig. 11 and the stress and plastic strain profiles in Fig. 14.

After generating the initial thermochemical state in a part (Fig. 15), a shot peening finite element simulation is performed with 12 impacts of a spherical shot on a semi-infinite plate as shown in Fig. 15. Using ABAQUS/Explicit, a symmetric model is used with a given choice for the sequences of the impacts on the surface. The 0.6-mm-diameter shot impacts the surface

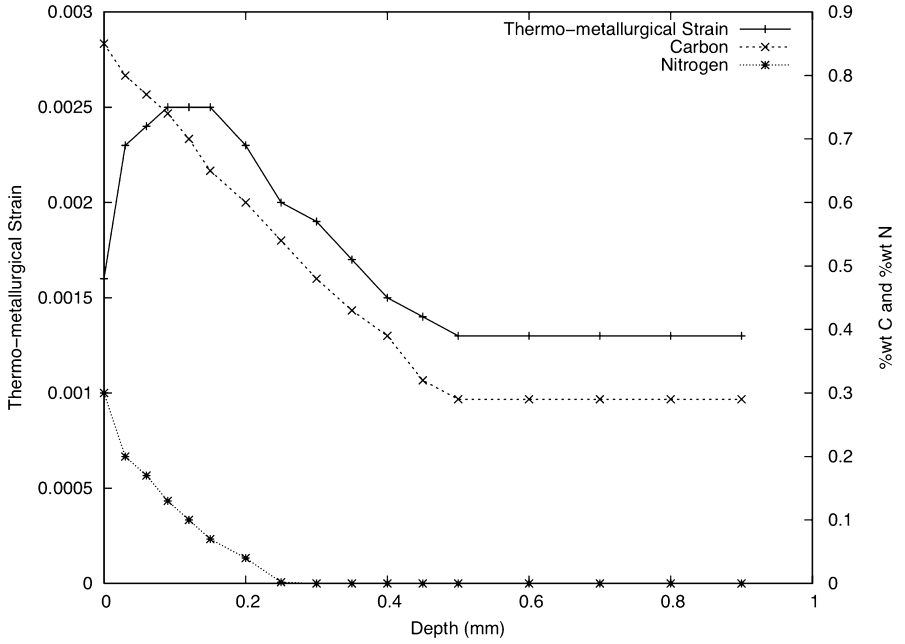

Fig. 13. Carbonitrided specimen: in-depth thermo-metallurgical strain profile (component *xx*) depending on the percentage of carbon and nitrogen at 25 °C (results obtained using JMatPro).

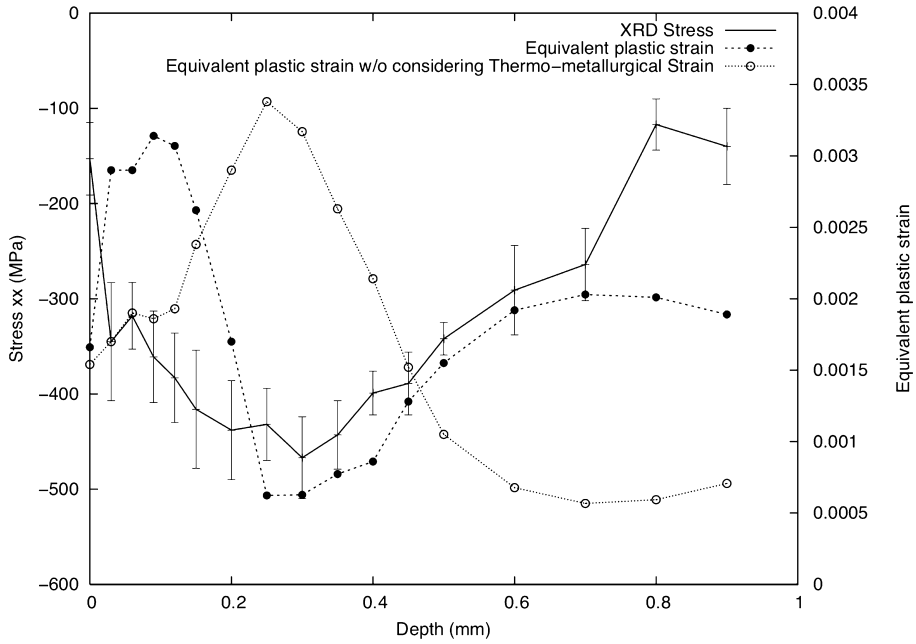

Fig. 14. Experimental residual stress profiles of carbonitrided 29MnCr5 Steel. Calculated equivalent plastic strain with and without considering thermo-metallurgical strains.

(90° angle) at a velocity of 55 m/s with a coverage of 110% as established by the experimental process [42]. The steel shot is modeled with spheres having an elastic isotropic behavior and the friction coefficient is constant and equal to 0.4. The material stress–strain hardening curves versus depth are given in Fig. 11 for carbonitriding. The same procedure has been applied by Renaud for carbonitriding and carburizing.

Fig. 16 presents the stress profiles along the depth for carburizing (a) and carbonitriding (b) prior to shot peening. Finite element stress profiles were compared to experimental ones. The stress profile was averaged over the area of the impacted zone (under the 12 impacts) at each depth.

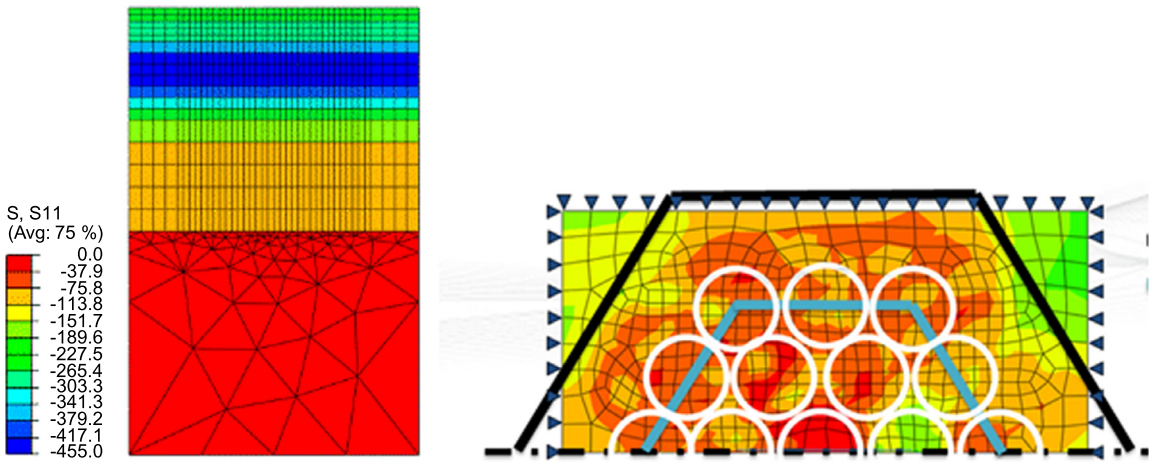

Fig. 15. Induced stress after carburizing (left) and shot peening finite element model with 12 spheres on a symmetric semi-infinite body (right).

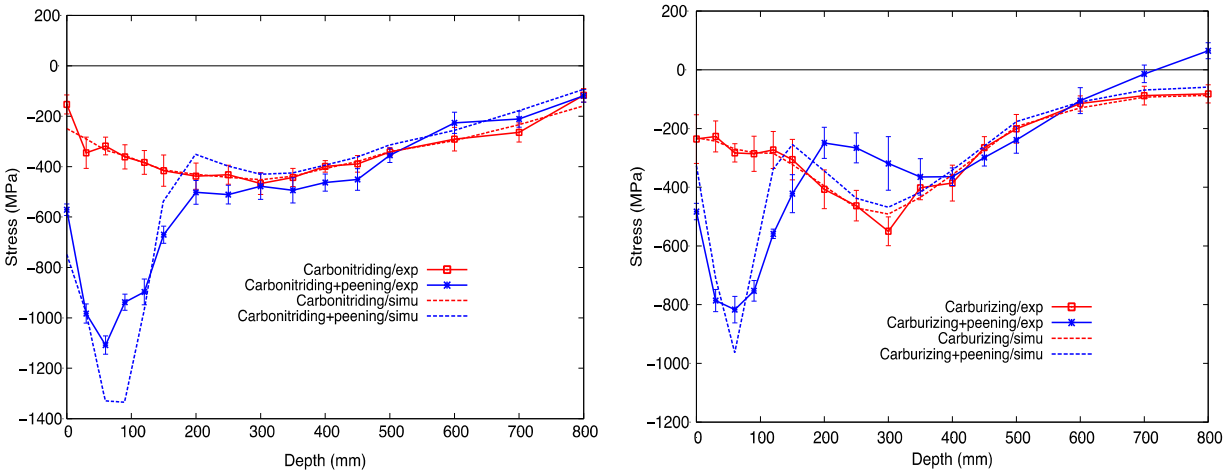

Fig. 16. Stress profiles after carburizing and after shot peening and after carbonitriding followed by shot peening – Experimental data obtained by XRD (solid lines) and results of finite element calculation (dashed lines).

Estimated stress profiles are in good agreement with experimental ones. More investigations are underway to analyze the effect of shot peening on the stability of the microstructure.

6.2. Shot peening models for complex geometries

There are several methods to determine residual stresses in a shot-peened part: it can be measured experimentally [12] or it can be simulated with analytical or numerical methods. Examples have been given in the previous sections. These methods predict the state of a shot-peened part considering that it is a semi-infinite body. There is a lack of available data in the literature concerning complex geometry issues and shot peening. An experimental analysis has nevertheless been proposed [45]. In order to dispose of reliable methods, we thus now consider the treatment of a part with a complex geometry. The residual stress field and the other material variable are expected to be affected by a strong local radius of curvature. The impact coverage during shot peening is directly related to the geometry. Also, the geometry modifies the stress equilibrium (compared to the case of a semi-infinite body). We thus wish to propose a finite element model of the shot peened part. One of the difficulty is to propose an adequate mesh of the structure, suitable to introduce shot-peening gradients. There is indeed a difficulty concerning the scales, and the mesh has to be adapted. Afazov et al. [46] propose an adapted methodology for this purpose.

We consider the case of the gear that is shot peened with ultrasonic shot peening as presented in Section 3. The analytical method proposed in Section 4.2 provides the residual stress field within a semi-infinite body made of the same material and for the impact velocities established in Section 3. The results are presented in Fig. 7. The associated plastic deformation field can be easily deduced (see Section 1). The geometry of the structure is modeled and meshed. The geometry has been simplified to consider that the tooth is a parallelepiped as presented in Fig. 17. The mesh has been created with elements

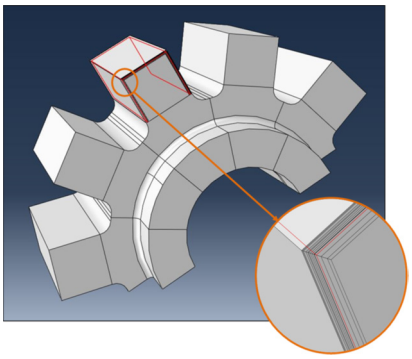

Fig. 17. Mesh and partition cells within the tooth gear adapted to the residual stress profile to be introduced.

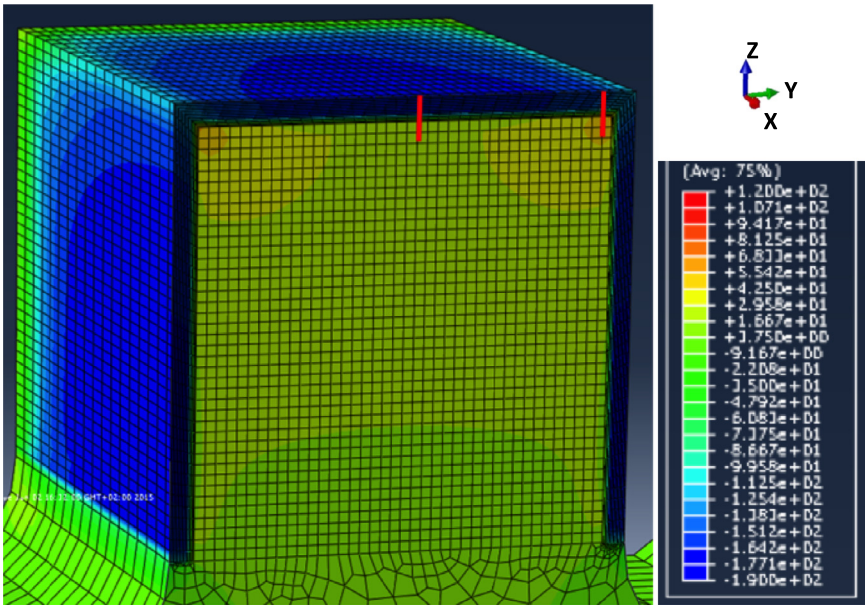

Fig. 18. Results of the finite-element analysis for the component σ_{xx} of the residual stress field.

having a size adapted to the local stress gradient close to the surface of the mechanical part (see Fig. 17). The plastic strain field found for the semi-infinite body is then introduced locally in a local coordinate system defined with the normal vector to the surface.

The results obtained after equilibrium are presented in Figs. 18 and 19. Fig. 18 presents the component σ_{xx} of the residual stress field expressed in the global coordinate system. Then, through thickness values are extracted along the two red paths presented in Fig. 18. The corresponding residual stress profiles are presented in Fig. 19 and compared with the residual stress profile that would be obtained in a semi-infinite body. In the middle of the tooth, the profiles are similar in shape, but the maximal value of the residual stress profile is reduced due to re-equilibrium. Close to the edge of the tooth the residual stress profile is completely modified. The stress field in the gear differs from the one that would be found in a semi-infinite body due to the presence of the edge. The complete stress field in the tooth is presented in Fig. 20. Clearly, the residual stress is complex, reaching positive values in some areas of the surface. Thus, even if the treatment is considered homogeneous and the surface regular such that the stress-free strains are close, locally, to the one that would be obtained in a semi-infinite body, the global equilibrium of the structure may change drastically the residual stress field. This could have major impacts on fatigue life prediction.

7. Conclusion

We have presented a convenient way to introduce an initial residual stress field due to shot peening within a complex geometry and have illustrated the methodology with the case of a gear. The proposed method enables us to obtain this result as a function of the process parameters when several models are chained together. The first step corresponds to the prediction of the shot dynamics as a function of the process parameters. This is an original method that enables us

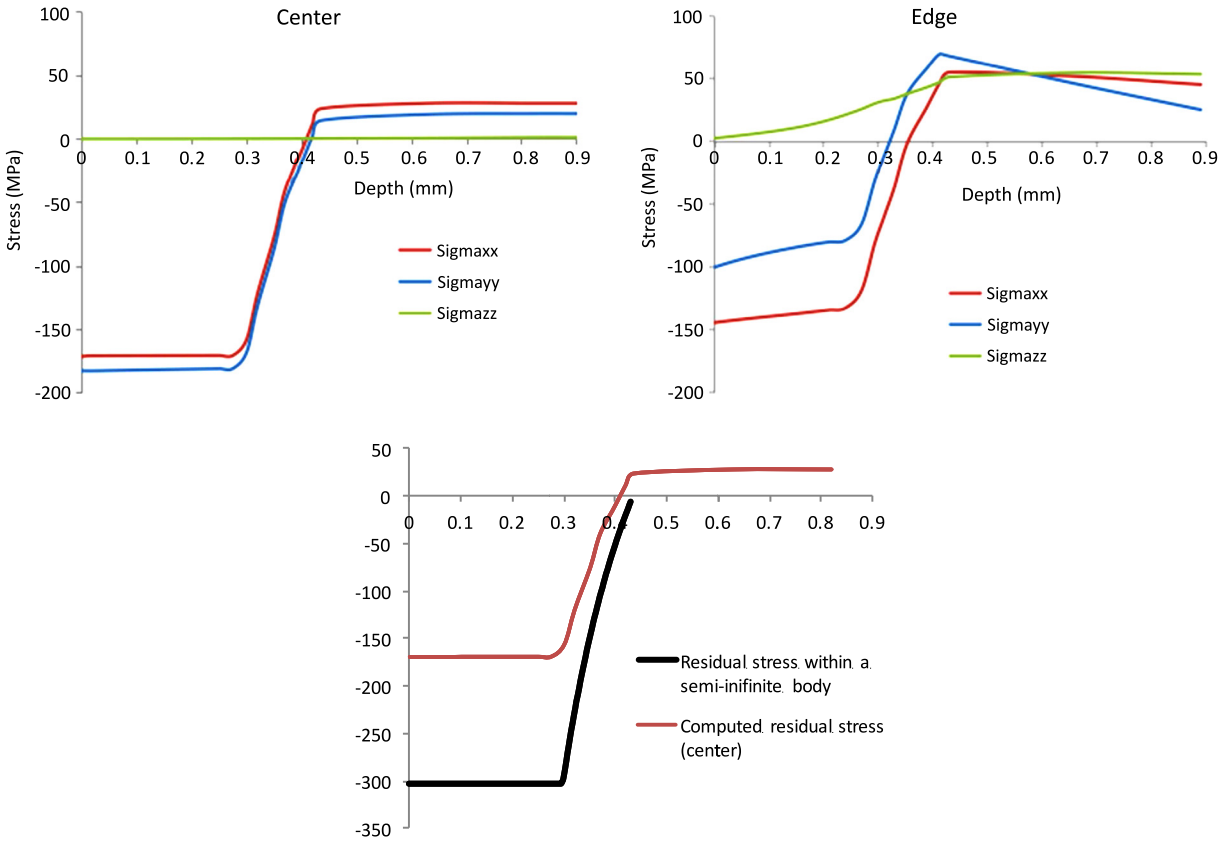

Fig. 19. Top: residual stress profiles as a function of the depth along the red lines represented in Fig. 11 and taken at the center of the tooth and close to its edge. Bottom: comparison of the residual stress field obtained in the middle of the tooth and the one obtained in a semi-infinite body treated with the same conditions as the gear.

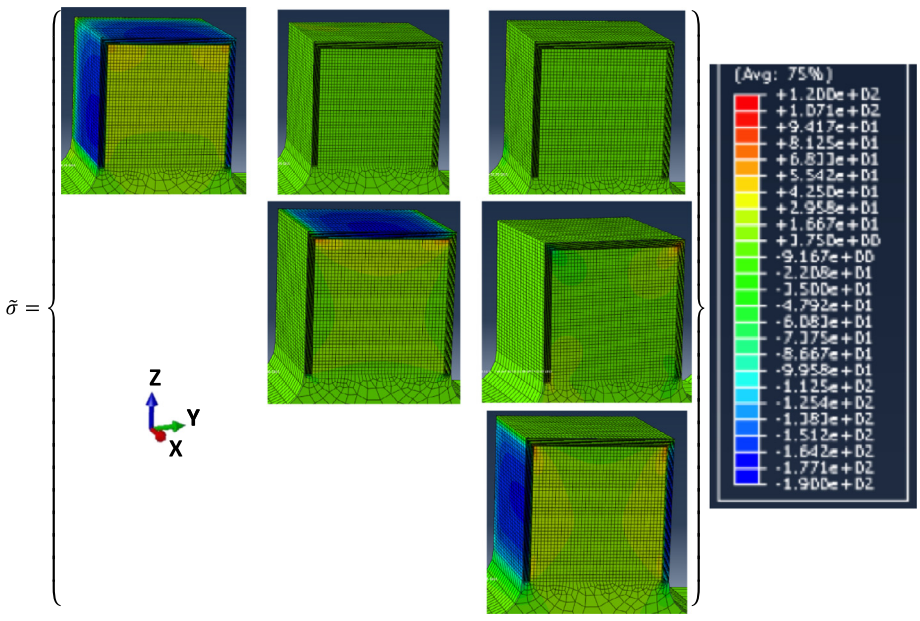

Fig. 20. Residual stress field within the tooth of a gear due to ultrasonic shot peening.

to optimize the process itself in terms of coverage and that gives the entire impact velocity field on a part with complex geometry. The residual stress field is then computed knowing the local impact velocity and can be implemented in a finite element model of a part with a complex geometry. A method to transfer the stress and plastic deformation fields due to shot peening into the geometry of the part has been discussed and is shown to be efficient. The proposed approach is consistent with industrial constraints in terms of computation time. The perspective is to complete the chaining process with fatigue life computations.

Acknowledgements

It is a pleasure to acknowledge the collaboration and financial support of SONATS Europe Technologies, the SAFRAN Group, PSA and the “Institut de recherche technologique Matériaux Métallurgie et Procédés”.

References

[1] J.O. Almen, Fatigue failures are tensile failures, Prod. Eng. 22 (1951) 101–124.
[2] J. Mackerle, FEM and BEM analysis and modeling of residual stresses: a bibliography, Finite Elem. Anal. Des. 37 (2001) 253–262.
[3] E. Rouhaud, D. Deslaef, J. Lu, J.-L. Chaboche, Modeling of residual stress, shot peening, in: Jian Lu (Ed.), Handbook on Residual Stress, Society of Experimental Mechanics, 2005.
[4] M. Zimmermann, M. Klemenz, V. Schulze, Literature review on shot peening simulation, Int J. Comput. Mater. Sci. Surf. Eng. 3 (4) (2010) 289–310.
[5] B. Bhuvaraghan, S. Srinivasan, B. Maffeo, Optimization of the fatigue strength of materials due to shot peening: a survey, Int. J. Struct. Chang. Solids, Mech. Appl. 2 (2010) 33–63.
[6] H. Wohlfart, The influence of peening conditions on the resulting distribution of residual stress, in: Proceedings of the 2nd International Conference on Shot Peening, Chicago, IL, USA, 1984.
[7] L. Barrallier, Genèse des contraintes résiduelles de nitruration: étude expérimentale et modélisation, Ph.D. thesis, ENSAM, 1992.
[8] J. Locquet, Caractérisations métallurgiques et mécaniques de couches nitrurées – relation microstructure–comportement, Ph.D. thesis, ENSAM, 1998.
[9] S. Jegou, L. Barrallier, R. Kubler, Residual stress generation in nitrided ternary Fe-3%Cr −0.345%C alloy: phase transformations induced residual stresses, Acta Mater. 58 (2010) 2666–2676.
[10] A. Sugianto, M. Narazaki, M. Kogawara, A. Shirayori, S.-Y. Kim, S. Kubota, Numerical simulation and experimental verification of carburizing-quenching process of SCr420H steel helical gear, J. Mater. Process. Technol. 209 (2009) 3587–3609.
[11] A.M. Korsunsky, On the modelling of residual stresses due to surface peening using eigenstrain distributions, J. Strain Anal. 40 (2005) 817–824.
[12] P.J. Withers, H.K.D.H. Bhadeshia, Residual stress, part I: measurement techniques, Mater. Sci. Technol. 17 (2001) 355–365.
[13] I. Altenberger, Mechanical surface treatment, shot peening, in: Jian Lu (Ed.), Handbook on Residual Stress, Society of Experimental Mechanics, 2005.
[14] J. Zarka, G. Inglebert, P. Kasmai-Navidi, A New Approach in Inelastic Analysis of Structures, CADLM, 1990.
[15] S. Bagherifard, R. Ghelichi, M. Guagliano, Numerical and experimental analysis of surface roughness generated by shot peening, Appl. Surf. Sci. 258 (2012) 6831–6840.
[16] K. Han, D. Peric', A.J.L. Crook, D.R.J. Owen, A combined finite/discrete element simulation of shot peening processes, parts I and II: studies on 2D interaction laws, Eng. Comput. 17 (2000) 593–620.
[17] B. Bhuvaraghan, S. Srinivasan, B. Maffeo, R. McLain, Y. Potdar, O. Prakash, Shot peening simulation using discrete and finite element methods, Adv. Eng. Softw. 41 (2010) 1266–1276.
[18] C. Nougier-Lehon, M. Zarwel, C. Diviani, D. Hertz, H. Zahouani, T. Hoc, Surface impact analysis in shot peening process, Wear 302 (2013) 1058–1063.
[19] T. Rousseau, T. Hoc, P. Gilles, C. Nouguier-Lehon, Effect of bead quantity in ultrasonic shot peening: surface analysis and numerical simulations, J. Mater. Process. Technol. 225 (2015) 413–420.
[20] K. Murugaratnam, S. Utili, A. Petrinic, A combined DEM–FEM numerical method for shot peening parameter optimisation, Adv. Eng. Softw. 79 (2015) 3–26.
[21] V.B. Nguyen, H.J. Poh, Y.-W. Zhang, Predicting shot peening coverage using multiphase computational fluid dynamics simulations, Powder Technol. 256 (2014) 100–112.
[22] M. Micoulaut, S. Mechkov, D. Retraint, P. Viot, M. François, Granular gases in mechanical engineering: on the origin of heterogeneous ultrasonic shot peening, Granul. Matter 9 (2007) 25–33.
[23] J. Badreddine, E. Rouhaud, M. Micoulaut, S. Remy, Simulation of shot dynamics for ultrasonic shot peening: the effects of process parameters, Int. J. Mech. Sci. 82 (2014) 179–190.
[24] J. Badreddine, S. Remy, M. Micoulaut, E. Rouhaud, V. Desfontaine, P. Renaud, CAD based model of ultrasonic shot peening for complex industrial parts, Adv. Eng. Softw. 76 (2014) 31–42.
[25] J. Badreddine, Modélisation du grenaillage ultrason pour des pieces à géométrie complexe, Thèse de Université de technologie de Troyes, 2014.
[26] A. Gariépy, S. Larose, C. Perron, M. Lévesque, Shot peening and peen forming finite element modeling – towards a quantitative method, Int. J. Solids Struct. 48 (2011) 2859–2877.
[27] H.Y. Miao, S. Larose, C. Perron, M. Lévesque, On the potential applications of a 3D random finite element model for the simulation of shot peening, Adv. Eng. Softw. 40 (2009) 1023–1038.
[28] K. Taehyung, Hyungyil Lee, Sunghwan Jung, Jin Haeng Lee, A 3D FE model for the evaluation of equi-biaxial peening residual stress due to multi-impacts, Surf. Coat. Technol. 206 (2012) 3981–3988.
[29] S.M.H. Gangaraj, M. Guagliano, G.H. Farrahi, An approach to relate shot peening finite element simulation to the actual coverage, Surf. Coat. Technol. 243 (2014) 39–45.
[30] S. Bagherifard, R. Ghelichi, M. Guagliano, On the shot peening surface coverage and its assessment by means of finite element simulation: a critical review and some original developments, Appl. Surf. Sci. 259 (2012) 186–194.
[31] T. Chaise, J. Li, D. Nélias, R. Kubler, S. Taheri, D. Douchet, V. Robin, P. Gilles, Modelling of multiple impacts for the prediction of distortions and residual stresses induced by ultrasonic shot peening (USP), J. Mater. Process. Technol. 212 (2012) 2080–2090.
[32] R. Comolet, J. Bonnin, Mécanique expérimentale des fluides, tome 2 et 3, 5e ed., Dunod, Paris, 2003.
[33] C. Ould, Analyse des contraintes résiduelles générées lors du grenaillage: approches analytique, numérique et expérimentale des impacts de billes, Thèse de doctorat de l'Université de technologie de Troyes, 2007.
[34] S. Baragetti, A. Terranova, Non-dimensional analysis of shot peening by means of DoE, Int. J. Mater. Prod. Technol. 15 (2000) 131–141.
[35] S. Baragetti, M. Guagliano, L. Vergani, Numerical procedure for shot peening optimization by means of non-dimensional factors, Int. J. Mater. Prod. Technol. 15 (2000) 131–141.

[36] D. Deslaef, Modélisation numérique du grenaillage de précontraintes: approche tridimensionnelle et dynamique, Thèse de doctorat de l'Université de technologie de Troyes, 2000.
[37] H. Guechichi, Prévision des contraintes résiduelles dues au grenaillage de précontrainte, Ph.D. thesis, ENSAM, 1986.
[38] S. Slim, Identification du comportement en plasticité et fatigue, influence du taux de recouvrement en grenaillage, Ph.D. thesis, ENSAM, 1995.
[39] M.T. Khabou, Modélisation du comportement et des contraintes résiduelles introduites dans un matériau soumis à un grenaillage, Ph.D. thesis, ENSAM, 1989.
[40] E. Rouhaud, A. Milley, J. Lu, Introduction of residual stress fields in finite element three-dimensional structures, in: Proceedings of the Fourth European Conference on Residual Stress, 1997.
[41] F. Ahdad, M. Desvignes, Contraintes résiduelles et déformations plastiques, leurs relations mutuelles pour les pièces de géométries simples, Matér. Tech. 5–6 (1996) 46–50.
[42] P. Renaud, Numerical simulations of the shot peening process of materials initially treated by carburizing or carbonitriding, Ph.D. thesis, Arts et Métiers ParisTech, 2011.
[43] X. Li, A. Miodownik, N. Saunders, Simultaneous calculation of mechanical properties and phase equilibria, J. Phase Equilib. 22 (2001).
[44] N. Saunders, Z. Guo, A. Miodownik, J.-P. Schille, Modelling the material properties and behaviour of multicomponent alloys, in: International Congress on FEM Technology with ANSYS CFX and ICEM CFD Conference, 2004.
[45] T.-S. Jun, A.M. Venter, A.M. Korsunsky, Inverse eigenstrain analysis of the effect of non-uniform sample shape on the residual stress due to shot peening, Exp. Mech. 51 (2011) 165–174.
[46] S.M. Afazov, A.A. Becker, T.H. Hyde, Mathematical modeling and implementation of residual stress mapping from microscale to macroscale finite element models, J. Manuf. Sci. Eng. 134 (2) (2012) 021001.